


## Article

# Characterization of Refining the Morphology of Al–Fe–Si in A380 Aluminum Alloy due to Ca Addition

Meng Wang , Yu Guo <sup>\*</sup>, Hongying Wang and Shengsheng Zhao

School of Mechanical and Electrical Engineering, Shenzhen Polytechnic, Shenzhen 518055, China; wanghy@szpt.edu.cn (H.W.); sszhao@szpt.edu.cn (S.Z.)

<sup>\*</sup> Correspondence: wangmeng04@szpt.edu.cn (M.W.); guoyu\_@szpt.edu.cn (Y.G.); Tel.: +86-185-6587-3580 (M.W.); +86-180-0453-7358 (Y.G.)

**Abstract:** Aluminum–silicon (Al–Si) alloys are the most commonly cast aluminum alloys. Fe is the most deleterious element for Al–Si die casting alloys, as its existence causes the precipitation of substantial intermetallics that result in the unsatisfactory mechanical performance of the alloy, such as its ductility. Hence, controlling the morphology and formation of the AlFeSi phase, particularly the  $\beta$ -AlFeSi phase, is vital for improving the ductility of Al–Si die casting alloys. Herein, Ca was added to the A380 alloy, and the morphological changes resulting from the influence of Ca on the AlFeSi phase were characterized. The outcomes revealed that according to different cooling rates, specific amounts of Ca addition (0.01–0.1 wt.%) were capable of refining  $\alpha$ -AlFeSi and  $\beta$ -AlFeSi morphology and transforming the  $\beta$ -AlFeSi phase into  $\alpha$ -AlFeSi. Moreover, Ca addition could also modify eutectic silicon. The transformation mechanism and refining role of Ca in AlFeSi and the different morphologies of  $\text{Al}_2\text{CaSi}_2$  were analyzed.

**Keywords:** A380 alloy; Ca; AlFeSi phase; refine



**Citation:** Wang, M.; Guo, Y.; Wang, H.; Zhao, S. Characterization of Refining the Morphology of Al–Fe–Si in A380 Aluminum Alloy due to Ca Addition. *Processes* **2022**, *10*, 672. <https://doi.org/10.3390/pr10040672>

Academic Editors: Guoqing Zhang and Prashant K Sarswat

Received: 24 January 2022

Accepted: 29 March 2022

Published: 30 March 2022

**Publisher's Note:** MDPI stays neutral with regard to jurisdictional claims in published maps and institutional affiliations.



**Copyright:** © 2022 by the authors. Licensee MDPI, Basel, Switzerland. This article is an open access article distributed under the terms and conditions of the Creative Commons Attribution (CC BY) license (<https://creativecommons.org/licenses/by/4.0/>).

## 1. Introduction

A380 aluminum alloy is one of the most extensively utilized Al–Si pressure casting alloys, and it is widely used in electronic and communicational devices, auto components, and engine parts.

For the majority of Al–Si die casting Al alloys, iron is a double-edged sword. In the presence of Fe, die soldering can be suppressed, whereas the fragile AlFeSi phase can affect the mechanical performance of Al–Si alloys in addition to causing a reduction in ductility. The existence of Fe induces the precipitation of Fe-rich intermetallics with platelet-like or fibrous morphologies, causing unsatisfactory mechanical performances of the overall alloy. Those intermetallics remarkably affect the tensile strength and plasticity of Al alloys by avoiding interdendritic feeding during the casting process and by causing the formation of numerous apertures in the eutectic phase. Thus, it is imperative to regulate the levels and morphologies of iron intermetallics in Al–Si compound metals to ensure optimal performance [1–6].

Among the iron-containing phases, the two most significant are the  $\beta$ -AlFeSi and  $\alpha$ -AlFeSi phases. The  $\beta$ -AlFeSi phase is harmful due to its platelet or needle-shaped morphology, which is fragile, and therefore, the alloy can be more severely influenced by the stress concentration. The crystal structure of  $\beta$ -AlFeSi is monoclinic, with lattice parameter  $a = b = 0.611$  nm,  $c = 4.15$  nm,  $\beta = 91^\circ$ . The  $\alpha$ -AlFeSi phase, which presents a certain compact morphological status, such as Chinese scripts, stars, or polygon shapes, is less deleterious to the material performance [7–9]. The crystal structure of  $\alpha$ -AlFeSi is cubic, with parameter  $a = 1.26$  nm. Hence, substantial amounts of research have been committed to reducing the fraction of  $\beta$ -AlFeSi, either directly or through conversion into  $\alpha$ -AlFeSi [10–13].

Thus, different approaches have been utilized to decrease the detrimental influence of AlFeSi intermetallic phases, including iron level reduction, element alloying, cooling rate control, and heat treatment. Among these approaches, element alloying is the most commonly used method, and many related studies have been conducted [9]. Mn possesses an atom lattice similar to Fe and can be used as an Fe substitute in  $\beta$ -AlFeSi to generate  $\alpha$ -Al(Mn,Fe)Si, which has the same lattice structure as  $\alpha$ -AlFeSi. Therefore, it can be used to reliably avoid the deleterious influence of  $\beta$ -AlFeSi. Nevertheless, Mn can facilitate the formation of primary  $\alpha$ -Al(Mn,Fe)Si precipitation in Al–Si cast alloys of a large size, resulting in the loss of ductility. Sr is another satisfactory Fe substitute, but its high cost and associated sintering challenges limit its usage. There are also other elements for alloying, while the effect still has limitations. [7,14–17]

Calcium can also act as a valid Fe substitute and functions via the refinement of the AlFeSi phase and the eutectic Si phase, improving the strength and ductility, particularly via elongation. Sreeja Kumari claimed that calcium supplementation could refine both eutectic Si and platelet Fe-intermetallic phases in Al–7Si–0.3Mg–0.6Fe alloy, which also enhanced the tensile properties and impacted the strength of the material [18,19]. Moreover, Ca can be combined with other elements, such as Be, Mn, and Sr, to mitigate the detrimental influence of the AlFeSi phase [20,21]. In a previous study, we found that the addition of Ca and Mn to the A380 alloy resulted in a microstructure consisting of FCC  $\alpha$ -Al, modified eutectic Si,  $\alpha$ -AlFeSi Chinese script phases, and refined platelet  $\beta$ -AlFeSi phase [21].

Nevertheless, comprehensive studies on the roles of Ca in Fe-rich phases of A380 alloy are insufficient. On the one hand, in previous studies, the content of Fe was comparably low, with low Ca addition (less than 0.01 wt.%). On the other hand, in die cast aluminum A380 alloy, a high level of Fe (about 1 wt.%) needs a high amount of Ca addition (even 0.3 wt.%) as a correction agent. In addition, the function of  $\text{Al}_2\text{CaSi}_2$  introduced by Ca addition has not been clearly illustrated. Therefore, in the present research, the roles of the Ca level and the cooling rates in the AlFeSi phase of A380 alloy were analyzed, and the findings can elucidate the mechanisms underlying Ca refinement of the AlFeSi phase.

## 2. Materials and Methods

In this study, three different cooling rates were studied. A copper mold with a V-shaped slope and a straight water quench method were used to emulate the high cooling rates of die casting. As per the secondary dendritic arm space identified, cooling rates around 50 °C/s were studied. A steel mold was employed to realize moderate cooling rates around 5 °C/s. Furnace cooling was utilized for low cooling rates at 0.05 °C/s. Moderate and low cooling rates were documented using National Instruments cDAQ-9171 data collection devices. The association between the secondary dendritic arm spacing ( $d$ ) and the relevant cooling velocity ( $t$ ) can be delineated by:

$$d = A \left( \frac{1}{t} \right)^n \quad (1)$$

As per the outcomes of Samuel [14],  $A$  and  $n$  are approximately 31 and  $-0.366$ , respectively. Hence, for the fast cooling rate samples, since the values of the secondary dendritic arm spacing were around 14  $\mu\text{m}$ , the cooling rates computed from Equation (1) for high-cooling-rate specimens were approximately 50 °C/s, which qualified our research design.

The sample utilized in this study was the commercially available Alcoa Al A380, which is a hypoeutectic aluminum with a comparatively low liquidus (593 °C) and solidus (527 °C) temperature. The A380 + Ca additive samples were fabricated from the master alloy. The constituents of the master alloy and the initial A380 are presented in Tables 1 and 2, respectively. The Ca additions were 0.01, 0.05, 0.1, and 0.3 wt.%.

**Table 1.** Composition of the master alloy.

| Material | Major    | Minor Element Composition (% by weight) |       |       |             |              | Al      |
|----------|----------|---|-------|-------|-------------|--------------|---------|
|          |          | Si                                      | Fe    | Mg    | Others Each | Others Total |         |
| Ca10     | Ca = 10% | ≤0.20                                   | ≤0.30 | ≤0.05 | ≤0.05       | ≤0.10        | Balance |

**Table 2.** Composition of the A380 alloy.

| Element | Si  | Fe  | Cu  | Mn  | Mg  | Ni  | Zn   | Ti   | Al      |
|---------|-----|-----|-----|-----|-----|-----|------|------|---------|
| wt.%    | 9.0 | 1.0 | 3.5 | 0.4 | 0.2 | 0.3 | 0.35 | 0.08 | Balance |

For the preparation of all the alloy specimens, the alloys were melted in a Kerl automatic standard electrical melt stove (Cincinnati, OH, USA). The cast metal for a single casting process was approximately 180 g. The melted alloys were held under 710 °C for 120 min and subjected to a slow cooling process until reaching the target temperature of 660 °C for casting.

The prepared specimens were sliced, milled, and subjected to careful polishing. The treated specimens were subjected to etching via a 0.5% HF in distilled water. Optical images were captured using a Leica DM LM/P 11888500 light microscope (Berlin, Germany). The SEM analyses were conducted via a Hitachi S-4800 field emission SEM (Tokyo, Japan) or an FEI Philips XL-40 SEM (Hillsboro, OR, USA).

### 3. Results

#### 3.1. A380–Ca Equilibrium Phase Diagram

The A380–Ca equilibrium phase diagram obtained by using Thermo-Calc is shown in Figure 1. From the phase diagram, it can be seen that if the Ca content is lower than 0.6 wt.%,  $\alpha$ -AlFeSi precipitates in advance of  $\beta$ -AlFeSi, and therefore no large primary  $\beta$ -AlFeSi can form. Therefore, the highest desired Ca addition is 0.6 wt.%. Additionally, the introduction of Ca can induce the formation of the  $\text{Al}_2\text{CaSi}_2$  phase, which can serve as a nucleation center for other secondary AlFeSi phases. Thus, from the calculated phase diagram, Ca addition may improve the ductility of the A380 alloy.

#### 3.2. The Effect of Ca Addition on the Morphology and Phase Fraction of A380 at Different Cooling Rates

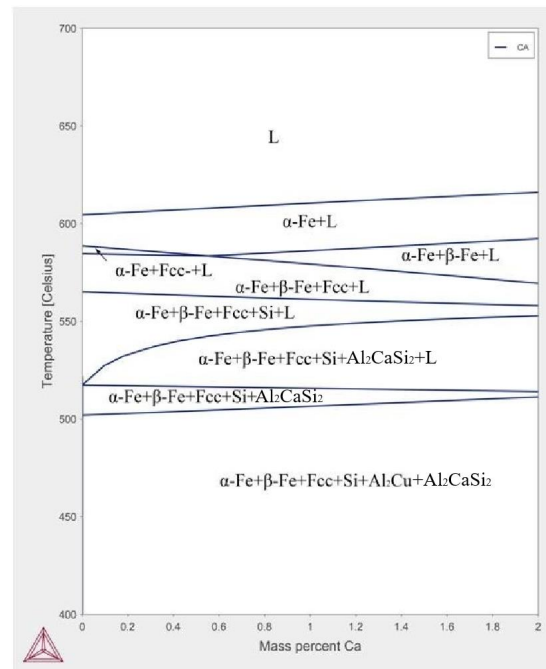
##### 3.2.1. Equilibrium Situation (Low Cooling Rate)

In the equilibrium situation, several phenomena were observed (Figure 2a–d): (1) No evident fraction change in the  $\beta$ -AlFeSi phase was observed. Nevertheless, the average size of the  $\beta$ -AlFeSi phase was reduced, and no primary  $\beta$ -AlFeSi phase was found if the Ca addition was higher than 0.05 wt.%, which revealed the refinement effect of Ca on the  $\beta$ -AlFeSi phase. (2) Polygon-shaped  $\text{Al}_2\text{CaSi}_2$  tended to occur under the low cooling rates when the Ca content was 0.1 wt.%, whereas no obvious  $\text{Al}_2\text{CaSi}_2$  was formed if the Ca content was lower than 0.1 wt.%. (3) Eutectic silicon became refined with the addition of Ca, with an obvious decrease in particle size observed. From the images, we can conclude that at a low cooling rate, Ca can reduce the size of the  $\beta$ -AlFeSi phase, and the best addition of Ca content is around 0.1 wt.%.

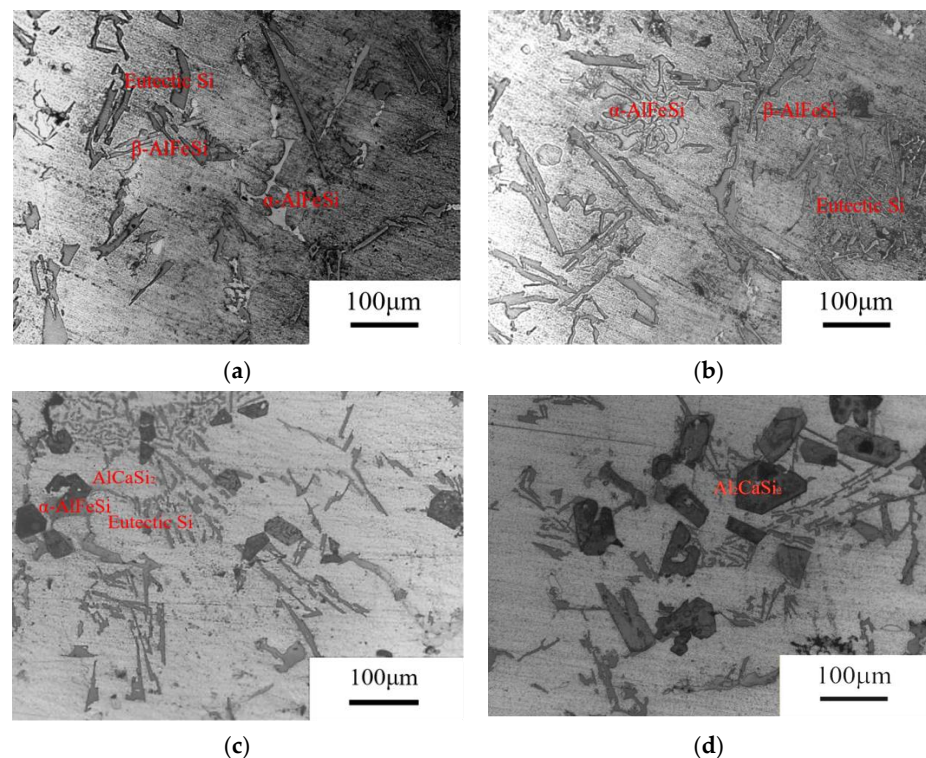
##### 3.2.2. Moderate Cooling Rates

Figure 3 shows the microstructure of the A380 alloy with different Ca additions at 5 °C/s. When the cooling rate was elevated, several other phenomena could be identified: (a) With an increase in Ca, the  $\beta$ -AlFeSi phase was transformed into an  $\alpha$ -AlFeSi phase. No evident variations were observed in the A380–0.01 Ca specimen (Figure 3a), whereas a noticeable decrease in the  $\beta$ -AlFeSi phase in the A380–0.05 Ca specimen was identified (Figure 3b). When the Ca level was higher than 0.05 wt.%, the  $\beta$ -AlFeSi phase was entirely

transformed into the  $\alpha$ -AlFeSi phase. (b) When the Ca level was 0.1 wt.%, a polygon-shaped  $\text{Al}_2\text{CaSi}_2$  phase formed (Figure 3c), while some needle-shaped  $\text{Al}_2\text{CaSi}_2$  were observed when the Ca addition level was up to 0.3 wt.%, which was detrimental to the performance of the alloy (Figure 3d). Thus, at a 5 °C/s cooling rate, 0.05 wt.% Ca addition is the optimal content.



**Figure 1.** Al-Si-Cu-xCa phase diagram (Si = 9%, Cu = 3.5%, Mn = 0.4%, Fe = 1%, Mg = 0.2%, Zn = 0.35%, and Al = balance).



**Figure 2.** Microstructure of the A380 alloy with different Ca additions at 0.05 °C/s cooling rate: (a) 0.01 wt.%; (b) 0.05 wt.%; (c) 0.1 wt.%; (d) 0.3 wt.%.



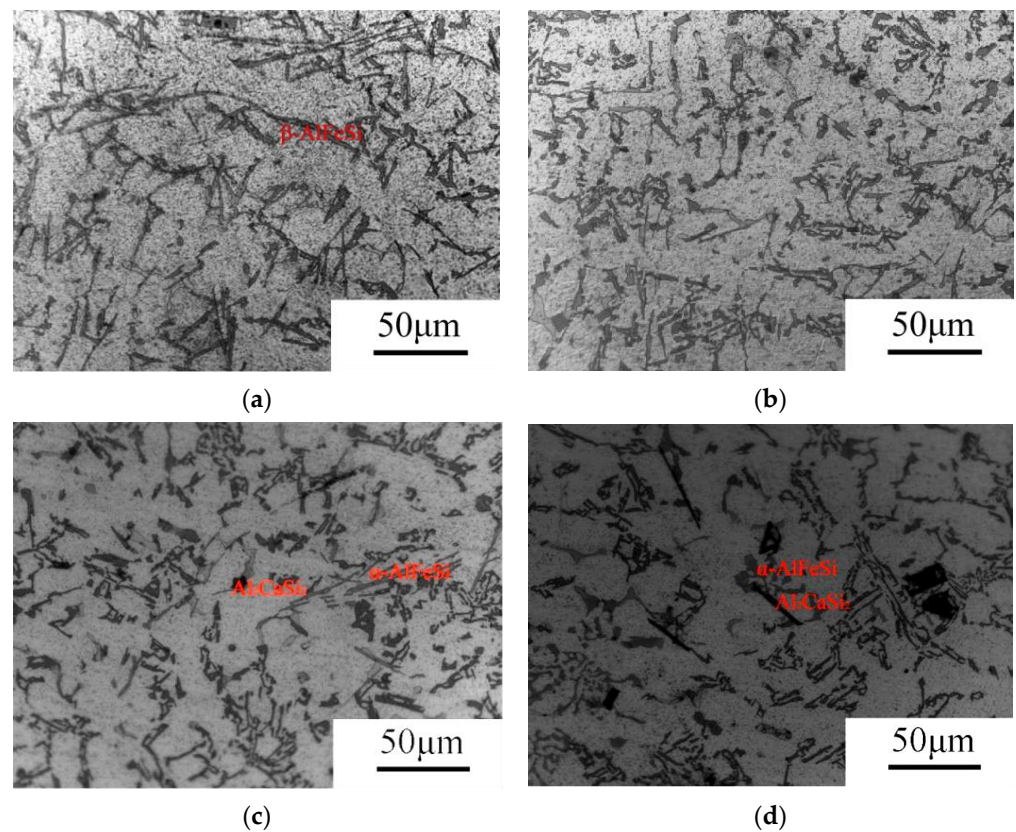


**Figure 3.** Microstructure of A380 alloy with different Ca additions at 5 °C/s cooling rate: (a) 0.01 wt.%; (b) 0.05 wt.%; (c) 0.1 wt.%; (d) 0.3 wt.%.

### 3.2.3. High Cooling Rates

When the cooling rate was increased even further to 50 °C/s, the AlFeSi phase was further refined under the influence of both the high cooling rates and Ca addition. Figure 4 shows the microstructure of the A380 alloy with diverse Ca levels at 50 °C/s. When Ca additions ranged from 0.01 to 0.05 wt.%, no large blocks of  $\alpha$ -AlFeSi and  $\beta$ -AlFeSi phases were found. Ca further modified the eutectic Si, and the morphology of the eutectic Si changed from a platelet morphology to a coral-like morphology. Thus, 0.01–0.05 wt.% Ca addition is enough for A380 alloy at a 50 °C/s cooling rate.

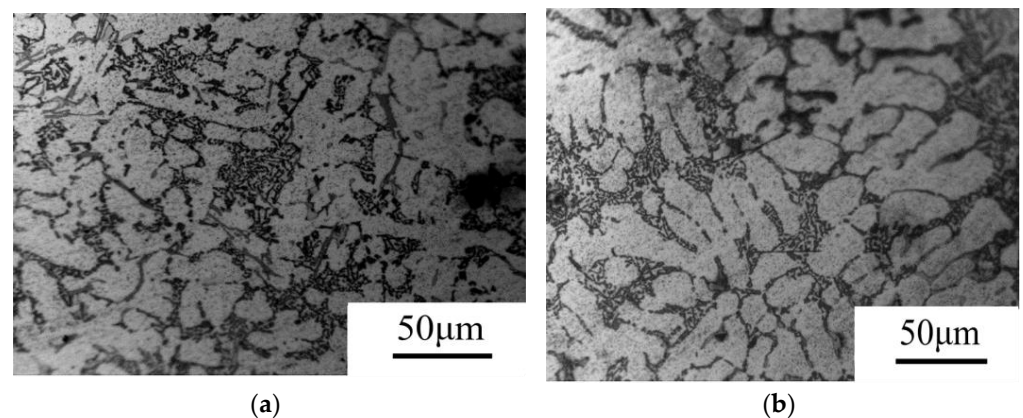


**Figure 4.** Microstructure of A380 alloy with different Ca additions at 50 °C/s cooling: (a) 0.05 wt.%; (b) 0.1 wt.%.

## 4. Discussion

### 4.1. The Refinement Effect of Ca on the AlFeSi Phase

There have been several studies on the mechanism of Ca in the AlFeSi phase. Kumari stated that the refining role of Ca in the  $\beta$ -AlFeSi phase was induced by the fragmented  $\beta$ -platelets. With the addition of Ca, he argued that the greater diffusion coefficient of Si relative to Fe could cause fragmentation of the  $\beta$ -AlFeSi-phase platelets due to the presence of Ca [18].

Low levels of Ca were associated with reductions in the particle size of  $\beta$ -AlFeSi, which coincided with the fragmentation theory. Nevertheless, when the Ca level reached 0.1 wt.%, more  $\alpha$ -AlFeSi was generated, and no evident  $\beta$ -AlFeSi was identified. Such a phenomenon cannot be sufficiently explained by the fragmentation theory but is possible based on the nucleation theory. Our team discovered that the  $\text{Al}_2\text{CaSi}_2$  phase was related to  $\alpha$ -AlFeSi. We identified that polygon-sized  $\alpha$ -AlFeSi were nucleated from the polygon-size  $\text{Al}_2\text{CaSi}_2$ , and  $\alpha$ -AlFeSi entirely wrapped the  $\text{Al}_2\text{CaSi}_2$  nucleating center, which was reported in our previous work (Figure 5a) [21]. In addition, the needle-shaped  $\text{Al}_2\text{CaSi}_2$  phase spread across the dendrites, which acted as the primary phase to generate  $\alpha$ -AlFeSi (Figure 5b). Although in the calculated phase diagram of Figure 1, primary  $\alpha$ -AlFeSi and  $\beta$ -AlFeSi formed prior to  $\text{Al}_2\text{CaSi}_2$  during the cooling process, secondary  $\alpha$ -AlFeSi grew from the  $\text{Al}_2\text{CaSi}_2$  phase and consumed the iron during the transformation of primary  $\beta$ -AlFeSi to secondary  $\alpha$ -AlFeSi. Thus, the function of  $\text{Al}_2\text{CaSi}_2$  can reduce the amount of  $\beta$ -AlFeSi and reduce the size of  $\beta$ -AlFeSi. Additionally, the  $\text{Al}_2\text{CaSi}_2$  phase was capable of nucleating other phases, such as Si and  $\text{Al}_2\text{Cu}$ .

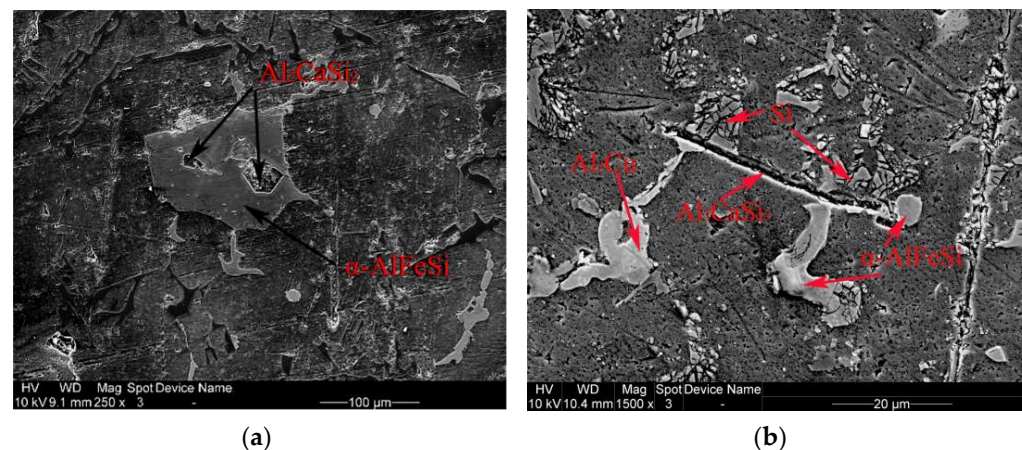


**Figure 5.** Relations of  $\text{Al}_2\text{CaSi}_2$  and  $\alpha$ -AlFeSi: (a) SEM images showing nucleation of  $\alpha$ -AlFeSi from polygon-shaped  $\text{Al}_2\text{CaSi}_2$ , retrieved from [21]; (b) SEM images showing nucleation of  $\alpha$ -AlFeSi from needle-shaped  $\text{Al}_2\text{CaSi}_2$ .

Intriguingly, we also discovered that  $\beta$ -AlFeSi could be thoroughly refined by  $\text{Al}_2\text{CaSi}_2$  at a high cooling rate (50 °C/s). The reason for this can be attributed to two factors: First, it is common knowledge that increasing cooling rates can both decrease the size of the AlFeSi phase and prompt the conversion of  $\beta$ -AlFeSi into  $\alpha$ -AlFeSi. The  $\beta$ -AlFeSi is a stable phase that can be generated at slow cooling rates, while  $\alpha$ -AlFeSi is a metastable phase. Second, in the equilibrium situation, the  $\text{Al}_2\text{CaSi}_2$  phase was generated subsequent to the formation of the primary AlFeSi phase. The high cooling rate postponed the forming temperature of the AlFeSi phase, whereas it played no role in the formation of the  $\text{Al}_2\text{CaSi}_2$  phase. Thereby, the  $\text{Al}_2\text{CaSi}_2$  phase could form first and directly nucleate  $\alpha$ -AlFeSi.

Another way to determine the validity of the nucleating AlFeSi phase in the nucleation substrate is to compute the planar disregistry  $\delta$ . As aforementioned, this is the only way of realizing the calculation in a quantitative way. Hence, it was utilized as the main

computation for the possible nucleation potential and was used to assess the experiment outcomes;  $\delta$  has been described in [22] as:

$$\delta_{(hkl)_s}^{(hkl)_n} = \sum_{i=1}^{i=3} \frac{|d_{(uvw)_s} \cos \theta - d_{(uvw)_n}|}{3} \times 100 \quad (2)$$

where  $(hkl)_s$  is the low-index plane of the substrate,  $(uvw)_s$  is the low-index orientation in  $(hkl)_s$ ,  $(hkl)_n$  is the low-index plane of the nucleated solid,  $(uvw)_n$  is the low-index orientation in  $(hkl)_n$ ,  $d_{(uvw)_n}$  is the interatomic spacing along  $(uvw)_n$ ,  $d_{(uvw)_s}$  is the interatomic spacing along  $(uvw)_s$ , and  $\theta$  is an angle between  $(uvw)_s$ . The crystalline structure of  $Al_2CaSi_2$  is hexagonal, with lattice parameters of  $a = 0.4130$  nm and  $c = 0.7145$  nm. The crystal structure of  $\alpha$ -AlFeSi is cubic, with the parameters of  $a = 1.26$  nm. Therefore, in Equation (2),  $s$  is for  $Al_2CaSi_2$  and  $n$  is for  $\alpha$ -AlFeSi, and all the parameters above can be calculated. Campbell [23] hypothesized that the electronic contribution to the interfacial energy was beneficial when  $\delta$  was below 12%. Table 3 presents the outcomes computed in this study for  $\delta$ , which show that  $Al_2CaSi_2$  is a satisfactory nucleation substrate of  $\alpha$ -AlFeSi, hence, revealing how Ca is capable of modifying  $\beta$ -AlFeSi.

**Table 3.** Planar disregistries between  $\alpha$ - $Al_2CaSi_2$  and  $\alpha$ -AlFeSi.  $s$  is for  $Al_2CaSi_2$  and  $n$  is for  $\alpha$ -AlFeSi.

| Match Planes     | [hkl] s                      | [hkl] n | d[hkl] s (nm) | d[hkl] n (nm) | $\theta$ | $\delta$ (Pct) |
|------------------|------------------------------|---------|---------------|---------------|----------|----------------|
| (0001)s / (001)n | $\overline{1}010$            | [100]   | 2.146011      | 2.53          | 0 deg    | 7.90           |
|                  | $\overline{5}410$            | [110]   | 3.651899      | 3.57796       | 4.10 deg |                |
|                  | $\overline{1}2\overline{1}0$ | [010]   | 2.700338      | 2.53          | 0 deg    |                |

#### 4.2. Ca Refinement Effect on Si

Although Al–Si alloy modification is usually realized via adding Na and Sr, Ca is also utilized as a modifier. From the experimental outcomes, we could clearly observe that the morphology of the eutectic structure of silicon changed from a coarse plate-like morphology to a coral or fibrous shape. There are several reports that Al–Si alloy modification could be achieved via adding Ca, and the duration times were longer than those for Sr and Mn addition.

There are several explanations for the refinement mechanism of Ca on eutectic silicon. The reason for the modification effect of Ca on those alloys was the destructive effects of active impurity particulates, which served as the nucleation center of eutectic Si in an unmodified alloy. Thus, greater undercooling was introduced, which induced the formation of a significant number of solidification centers of Si, refining the eutectic silicon. Ca can also be adsorbed on the small crystals of eutectic Si to slow down their growth [24].

Another explanation is impurity-induced twinning. The addition of elements into molten alloys that contain Si can facilitate a transition of the morphology of the Si phase via the formation of growth twins. A modifier of an appropriate atom size (with respect to Si ( $r_{\text{modifier}}/r_{\text{silicon}} = 1.646$ ), upon incorporation into the molten alloy, can accumulate adequately via inducing growth twins for Si 3D growth. The radius ratio reported for Ca is 1.68, very close to 1.646 [25].

In our study, Ca introduced greater undercooling, which could spontaneously increase the formation of nucleation centers of Si. In addition, a growth twin was created with the absorbed Ca on the liquid/solid interface of Si, contributing to the modification of the Al–Si alloy upon Ca addition.

Moreover, higher cooling rates facilitated further refinement, whereas it could be clearly seen that the high cooling rate was responsible for refinement rather than modification by merely introducing additional Si nucleation centers.

It has also been previously reported that Ca could facilitate the formation of primary  $Al_2CaSi_2$ , which could serve as the nucleation substrate of primary Si [25]. Hence, we can conclude that both Ca and  $Al_2CaSi_2$  can refine eutectic silicon.



#### 4.3. $\text{Al}_2\text{CaSi}_2$ Morphology

As shown in the SEM images in Figure 5, two morphologies of  $\text{Al}_2\text{CaSi}_2$  were formed in our experiment. The first was polygon-shaped, which could be observed at low cooling rates. The second was needle-shaped, which could be observed at high cooling rates. The reason for this is that the crystalline structure of  $\text{Al}_2\text{CaSi}_2$  is hexagonal, with the lattice parameters of  $a = 0.4130 \text{ nm}$  and  $c = 0.7145 \text{ nm}$ . Therefore, at low cooling rates, growth occurred in a 3D manner, whereas at high cooling rates, there was no time for  $c$ -axis growth, and hence, growth proceeded in a 2D manner. Nevertheless, in both cases, they can serve as a nucleation substrate for  $\alpha$ -AlFeSi. Hence, it can reduce the fraction of  $\beta$ -AlFeSi.

In summary, the scheme of the relation of nucleation by polygon- and needle-shaped  $\text{Al}_2\text{CaSi}_2$  is shown in Figure 6. In Figure 6a, polygon-shaped  $\text{Al}_2\text{CaSi}_2$  can serve as the nucleate center of secondary  $\alpha$ -AlFeSi, and the formed  $\alpha$ -AlFeSi entirely trapped the polygon-shaped  $\text{Al}_2\text{CaSi}_2$  nucleate center. In Figure 6b, needle-shaped  $\text{Al}_2\text{CaSi}_2$  can serve as a dendrite nucleate origin of secondary  $\alpha$ -AlFeSi, ball shape  $\text{Al}_2\text{Cu}$ , and particulate silicon. All three phases grow outside of the needle-shaped  $\text{Al}_2\text{CaSi}_2$ .

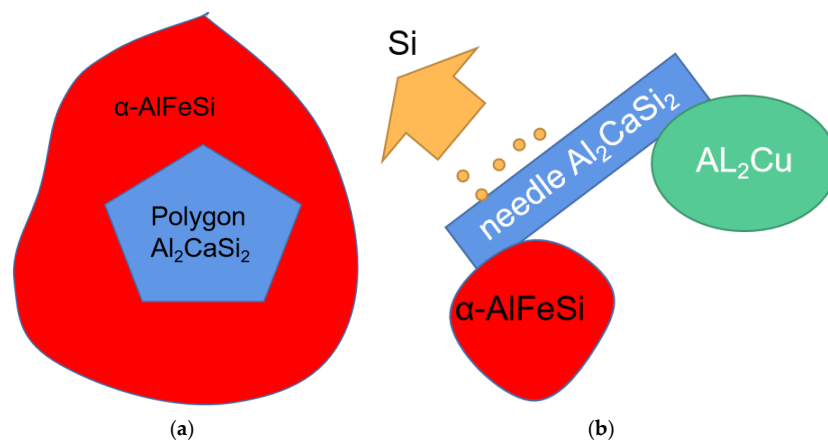


**Figure 6.** Relation of nucleation by (a) polygon- and (b) needle-shaped  $\text{Al}_2\text{CaSi}_2$ .

#### 5. Conclusions

- (1) Ca can accelerate the fragmentation of the  $\beta$ -AlFeSi phase and introduce  $\text{Al}_2\text{CaSi}_2$ , which acts as the nucleation substrate of  $\alpha$ -AlFeSi. At a low cooling rate,  $\text{Al}_2\text{CaSi}_2$  can transform primary  $\beta$ -AlFeSi to secondary  $\alpha$ -AlFeSi. At a high cooling rate, primary  $\text{Al}_2\text{CaSi}_2$  can directly nucleate secondary  $\alpha$ -AlFeSi.
- (2) A high cooling rate can facilitate the transformation of  $\beta$ -AlFeSi to  $\alpha$ -AlFeSi with lower Ca addition. Therefore, the best Ca addition for A380 alloy at the cooling rates of 0.05, 5, and 50  $^{\circ}\text{C/s}$  are 0.1 wt.%, 0.05 wt.%, and 0.01 wt.%, respectively.
- (3) Ca itself and  $\text{Al}_2\text{CaSi}_2$  can serve as the modification agents of eutectic silicon, and high cooling rates can only refine eutectic Si.
- (4) At low cooling rates, polygon-shaped  $\text{Al}_2\text{CaSi}_2$  form in a 3D growth manner, while at high cooling rates, needle-shaped  $\text{Al}_2\text{CaSi}_2$  form in a 2D growth manner, and both can serve as a nucleation substrate for  $\alpha$ -AlFeSi.

**Author Contributions:** Conceptualization, M.W. and Y.G.; methodology, M.W.; experiment, M.W.; validation, S.Z. and H.W.; writing—original draft preparation, M.W.; writing—review and editing, M.W.; funding acquisition, M.W., H.W. and S.Z. All authors have read and agreed to the published version of the manuscript.

**Funding:** This research was funded by the Post-Doctoral Later-Stage Foundation Project of Shenzhen Polytechnic (6020271008K), the Young Innovative Talents Project of General Colleges and Universities in Guangdong Province (2019GKQNCX127), the Shenzhen Science and Technology Project (JCYJ20190809150001747), and the Key Project of Shenzhen Polytechnic (6020310007K).



**Institutional Review Board Statement:** Not applicable.

**Informed Consent Statement:** Not applicable.

**Data Availability Statement:** Not applicable.

**Conflicts of Interest:** The authors declare no conflict of interest.

## References

- Ren, J.; Fang, X.; Chen, D. The effect of heat treatments on the microstructural evolution of twin-roll-cast Al-Fe-Si alloys. *J. Mater. Eng. Perform.* **2021**, *30*, 4401–4410. [\[CrossRef\]](#)
- Li, G.; Qu, W.-Y.; Luo, M.; Cheng, L.; Guo, C.; Li, X.-G.; Xu, Z.; Hu, X.-G.; Li, D.-Q.; Lu, H.-X.; et al. Semi-solid processing of aluminum and magnesium alloys: Status, opportunity, and challenge in China. *Trans. Nonferrous Met. Soc. China* **2021**, *31*, 3255–3280. [\[CrossRef\]](#)
- Liu, X.; Jia, H.-L.; Wang, C.; Wu, X.; Zha, M.; Wang, H.-Y. Enhancing mechanical properties of twin-roll cast Al-Mg-Si-Fe alloys by regulating Fe-bearing phases and macro-segregation. *Mater. Sci. Eng. A* **2021**, *831*, 142256. [\[CrossRef\]](#)
- Bardziński, P.J. New Al<sub>3</sub>Si<sub>7</sub> phase with tetragonal silicon structure in quasicrystal-forming near-eutectic Al-Cu-Fe-Si alloys. *J. Alloy. Compd.* **2021**, *869*, 159349. [\[CrossRef\]](#)
- Gan, J.; Du, J.; Wen, C.; Zhang, G.; Shi, M.; Yuan, Z. The Effect of Fe Content on the Solidification Pathway, Microstructure and Thermal Conductivity of Hypoeutectic Al-Si Alloys. *Int. J. Met.* **2021**, *16*, 178–190. [\[CrossRef\]](#)
- Gao, T.; Li, Z.; Zhang, Y. Phase Evolution of  $\beta$ -Al<sub>5</sub>FeSi During Recycling of Al-Si-Fe Alloys by Mg Melt. *Int. J. Metalcast.* **2019**, *13*, 473–478. [\[CrossRef\]](#)
- Lu, L.; Dahle, A.K. Iron-rich intermetallic phases and their role in casting defect formation in hypoeutectic Al-Si alloys. *Metall. Mater. Trans. A* **2005**, *36*, 819–835.
- Dinnis, C.M.; Taylor, J.A.; Dahle, A.K. As-cast morphology of iron-intermetallics in Al-Si foundry alloys. *Scr. Mater.* **2005**, *53*, 955–958. [\[CrossRef\]](#)
- Zhang, L.; Gao, J.; Damoah, L.; Robertson, D.G. Removal of Iron From Aluminum: A Review. *Miner. Process. Extr. Met. Rev.* **2012**, *33*, 99–157. [\[CrossRef\]](#)
- Becker, H.; Bergh, T.; Vullum, P.E.; Leineweber, A.; Li, Y. Effect of Mn and cooling rates on  $\alpha$ -,  $\beta$ - and  $\delta$ -Al-Fe-Si intermetallic phase formation in a secondary Al-Si alloy. *Materialia* **2019**, *5*, 100198. [\[CrossRef\]](#)
- Becker, H.; Bergh, T.; Vullum, P.; Leineweber, A.; Li, Y.  $\beta$ - and  $\delta$ -Al-Fe-Si intermetallic phase, their intergrowth and polytype formation. *J. Alloy. Compd.* **2019**, *780*, 917–929. [\[CrossRef\]](#)
- Zhu, Y.Z.; Peng, H.; Huang, H.; Li, J.C. Abnormal Grain Growth Mechanism in the Twin-Roller Cast Al-Fe-Si Alloy in the Annealing Process. *Adv. Mater. Sci. Eng.* **2020**, *2020*, 1056274. [\[CrossRef\]](#)
- Gao, T.; Li, Z.-Q.; Liu, X.-F.; Zhang, Y.-X. Evolution Behavior of  $\gamma$ -Al<sub>3.5</sub>FeSi in Mg Melt and a Separation Method of Fe from Al-Si-Fe Alloys. *Acta Met. Sin. Engl. Lett.* **2017**, *31*, 48–54. [\[CrossRef\]](#)
- Samuel, M.; Samuel, F.H. Effect of alloying elements and dendrite arm spacing on the microstructure and hardness of an Al-Si-Cu-Mg-Mg-Fe-Mn (380). *J. Mater. Sci.* **1995**, *301*, 1698–1708. [\[CrossRef\]](#)
- Wang, M.; Xu, W.; Han, Q.Y. Effect of heat treatment on controlling the morphology of AlFeSi phase in A380 alloy. *Int. J. Metalcast.* **2016**, *10*, 516–523. [\[CrossRef\]](#)
- Wang, M.; Xu, W.; Han, Q. The Influence of Sr Addition on the Microstructure of A380 Alloy. *Int. J. Met.* **2017**, *11*, 321–327. [\[CrossRef\]](#)
- Wang, P.; Deng, Y.; Dai, Q.; Jiang, K.; Chen, J.; Guo, X. Microstructures and strengthening mechanisms of high Fe containing Al-Mg-Si-Mn-Fe alloys with Mg, Si and Mn modified. *Mat. Sci. Eng. A-Struct.* **2021**, *803*, 140477. [\[CrossRef\]](#)
- Kumari, S.S.; Pillai, R.; Pai, B. A study on the structural, age hardening and mechanical characteristics of Mn and Ca added Al-7Si-0.3Mg-0.6Fe alloy. *J. Alloy. Compd.* **2008**, *453*, 167–173. [\[CrossRef\]](#)
- Kumari, S.S.; Pillai, R.; Rajan, T.; Pai, B. Effects of individual and combined additions of Be, Mn, Ca and Sr on the solidification behaviour, structure and mechanical properties of Al-7Si-0.3Mg-0.8Fe alloy. *Mater. Sci. Eng. A* **2007**, *460–461*, 561–573. [\[CrossRef\]](#)
- Belov, N.; Naumova, E.; Akopyan, T. Effect of 0.3% Sc on microstructure, phase composition and hardening of Al-Ca-Si eutectic alloys. *Trans. Nonferrous Met. Soc. China* **2017**, *27*, 741–746. [\[CrossRef\]](#)
- Wang, M.; Xu, W.; Han, Q. Study of Refinement and Morphology Change of AlFeSi Phase in A380 Alloy due to Addition of Ca, Sr/ Ca, Mn and Mn, Sr. *Mater. Trans.* **2016**, *57*, 1509–1513. [\[CrossRef\]](#)
- Cao, X.; Campbell, J. Morphology of Beta-Al<sub>5</sub>FeSi Phase in Al-Si Cast Alloys. *Mater. Trans.* **2006**, *4*, 1303–1312. [\[CrossRef\]](#)
- Campbell, J. *Casting*; Butterworth-Heinemann: Oxford, UK, 1991.
- Korotkova, N.O.; Belov, N.A.; Avxentieva, N.N. Effect of Calcium additives on the phase composition and physicomechanical properties of a conductive alloy Al-0.5% Fe-0.2% Si-0.2% Zr-0.1% Sc. *Phys. Met. Metallogr.* **2020**, *121*, 95–101. [\[CrossRef\]](#)
- Kumari, S.S.S.; Pillai, R.M.; Pai, B.C. Role of calcium in aluminium based alloys and composites. *Int. Mater. Rev.* **2005**, *50*, 216–238. [\[CrossRef\]](#)